Paracetamol removal by Kon-Tiki kiln-derived biochar and activated carbons

A.L. Bursztyn Fuentes, Rafael Luan Sehn Canevesi, Philippe Gadonneix, Sandrine Mathieu, Alain Celzard, V. Fierro

Paracetamol removal by Kon-Tiki kiln-derived biochar and activated carbons

A. L. Bursztyn Fuentes[1], R. L. S. Canevesi[2], P. Gadonneix[2], S. Mathieu[3], A. Celzard[2], V. Fierro[2*]

[1] Centro de Tecnología de Recursos Minerales y Cerámica (CETMIC) CIC - CONICET La Plata, Centenario y 506, M. B. Gonnet, Argentina

[2] Université de Lorraine, CNRS, IJL, F-88000 Epinal, France

[3] Université de Lorraine, CNRS, IJL, F-54000 Nancy, France

[*] Corresponding author. Tel: + 33 329 29 61 77. Fax: + 33 329 29 61 38. E-mail address : Vanessa.Fierro@univ-lorraine.fr (V. Fierro)

Abstract

Biochar was obtained from Eucalyptus pruning residues with a non-conventional device named Kon-Tiki kiln. The average heat of combustion of the biochar, 27.3 MJ kg^{-1}, was higher than that of Eucalyptus wood, 17.8 MJ kg^{-1}. Activation with CO_2 was performed by varying the activation time from 0 to 60 minutes. The activated carbons (ACs) and the carbon precursor have been characterised and tested for paracetamol removal in the liquid phase, studied in both kinetic and equilibrium aspects. ACs presented an increase in BET area (up to 845 m^2/g), total pore volume and microporosity with the activation time. The pseudo-second order model was the one that best fitted the experimental data. Elimination of paracetamol was much faster when using ACs, 5h, than when using the biochar, 3 days. However, pollutant removal was greater than 95% for all materials, which is a promising result for low-cost biochars in a difficult economic context. All the adsorption equilibrium experiments exhibited multilayer behaviour, showing values up to 98 mg g^{-1} for the maximum monolayer-adsorption capacity.

Keywords: Kon-Tiki kiln; activated carbon; biochar; CO_2 activation; paracetamol adsorption.

1. Introduction

Pharmaceutical and Personal Care Products (PPCPs) are emerging pollutants, which are increasingly found in treated urban and industrial wastewaters, as well as in watercourses (Kolpin et al., 2002). PPCPs are not listed as pollutants in the World Health Organization guidelines for drinking water quality (WHO, 2004) and, therefore, they are not regulated. For this reason, studies on their effects on human and environmental health are still rare (Daughton and Ternes, 1999). Although PCPCs are present in low concentrations in aquatic ecosystems, typically at trace levels (ng L^{-1} to μg L^{-1}), they can still induce adverse effects due to cumulative effects and continuous exposure (Boudrahem et al., 2017; Dordio et al., 2009).

Paracetamol (N-4-hydroxyphenylacetamide or acetaminophen), a common analgesic and anti-inflammatory for humans and animals, is usually chosen as a model molecule (García-Mateos et al., 2015; Lladó et al., 2015; Mestre et al., 2015, 2011; Spessato et al., 2020; Terzyk, 2001; Terzyk et al., 2003; Terzyk and Rychlicki, 2000) because it is a pharmaceutical compound used worldwide and does not require medical prescription. Depending on the source, 58 to 90% of the ingested paracetamol and its metabolites are excreted by the human body without being metabolised (Correia et al., 2016; Wu et al., 2012). In surface waters, the median concentration of paracetamol detected was 0.055 ± 0.051 μg L^{-1} (Bound and Voulvoulis, 2006; Gros et al., 2006; Wiegel et al., 2004) although higher concentrations have been measured. Paracetamol has been found in concentrations up to 6 μg L^{-1} in effluents from European sewage treatment plants, up to 10 μg L^{-1} in USA natural waters, and higher than 65 μg L^{-1} in the Tyne River in the UK (Wu et al., 2012). In raw wastewater, paracetamol was detected at a median concentration of 48 ± 75 μg L^{-1} but in raw hospital effluents and some wastewater effluents, paracetamol concentrations can even exceed 150 μg L^{-1} (Wu et al., 2012).

Activated carbons (ACs) have been widely studied to remove contaminants from water, and PPCPs are no exception (Acosta et al., 2016; Baccar et al., 2012; Marques et al., 2017; Mestre et al., 2009, 2007; Selmi et al., 2018). Pyrolysis of biomass at the laboratory scale for the production of ACs requires specific and expensive equipment both for carbonisation and activation steps. Commercial carbons are usually physically activated with steam, CO_2, air or mixtures, or are chemically activated by adding zinc salts, KOH or H_3PO_4 to the carbon precursors (Zhang et al., 2004). After chemical activation, an extensive washing step with water and sometimes HCl is needed (Fierro et al., 2006; Schaefer et al., 2016). Despite the desired chemical and textural properties are successfully achieved by chemical or physical activation, the overall yield of the process is sometimes quite low, especially by KOH activation (Basta et al., 2009; Szczurek et al., 2014).

This study focuses on the development of low-cost adsorbent production strategies. In this sense, Schmidt and Taylor designed a non-conventional carbonisation device named Kon-Tiki kiln, which allows the production of large amounts of carbonaceous material with minimal infrastructure and without external energy supply, promoting the reuse of agricultural by-products (Schmidt and Taylor, 2014). It follows the principle of pyrolysis of biomass layer after layer in an open metal kiln, conical in shape, easy to use, fast and resulting in low greenhouse gas emissions (Cornelissen et al., 2016). The process of carbonisation using this device resembles the carbon production by ancient civilisations and small contemporary communities, which proves that it is well known, easy to reproduce and cheap. Kon-Tiki kiln-derived biochar has been used for soil amendment as it possesses chemical properties and agronomic effects similar to those seen for biochars produced in other types of kilns (Pandit et al., 2017).

The aim of this study was to produce biochar from Eucalyptus pruning residues in a Kon-Tiki kiln and to use them *as such* or more carbonised and activated with CO_2, for the removal of paracetamol removal in water.

2. Materials and Methods

2.1 Biochar and activated carbons (ACs) preparation

Biochar was obtained from the urban pruning of Eucalyptus branches from La Plata, Argentina. Charring was performed in a Kon-Tiki kiln according to the procedure presented by Schmidt & Taylor (2014). In short, fire was first produced inside the kiln with small branches (diameter *d* about 1 cm) and, as soon as a layer of ash was perceived, new larger branches were added to the kiln (d < 4 cm). The kiln was fed constantly using the same criteria until all the selected biomass was consumed. Apart from the addition of more feedstock when the flames are low, the temperature in the Kon-Tiki kiln cannot be controlled, but the operating and investment costs are much lower than those of traditional carbonisation kilns. The maximum temperature recorded before quenching was 700ºC and was measured by using a copper-aluminium K-type thermocouple sheathed in an alumina tube and coupled to a digital thermometer. Figure SI 1 shows an image of the device in operation. Then, distilled water was poured to put out the fire. The biochar thus obtained was then filtered and dried at 105°C for 48h. The biochar was ground and sieved, and the particle fraction used in this study was 600-250 µm (mesh 30-60, ASTM). The material was labelled as CV.

Physical activation with CO_2 was carried out in a quartz tube reactor installed in a horizontal furnace. The inner diameter of the quartz tube was 3.5 cm and its length was 100 cm. A quartz boat containing between 0.5 and 0.6 g of CV was located in the centre of the quartz tube and the system was purged for 1 h with a 100 mL min^{-1} nitrogen flow to eliminate

any trace of oxygen before heating. Then, the oven was heated at 5°C min^{-1} to 900°C, and the latter temperature was held for 1h. Then, the nitrogen flow was switched to a 25 mL min^{-1} CO_2 flow, which was maintained for a given time of 15, 30 or 60 min. After this time, the sample was cooled under N_2 flow. The resultant activated carbons (ACs) were labelled as CV15, CV30 and CV60, respectively. The ACs obtained were weighed and the yield of the process (*Y*) was calculated according to equation (1):

$$Y = \frac{W_C}{W_{CH}} \times 100 \quad (1)$$

where W_{CH} is the initial weight of biochar and W_C is the weight of the sample after activation. A reference carbon material was prepared by heating CV up to 900°C for 1h without CO_2 activation and it was labelled CV0.

2.2 Materials characterisation

Carbon, hydrogen, nitrogen and sulphur contents in all carbonaceous materials were determined using an elemental analyser (Vario El Cube, Elementar). Oxygen was also determined in the same equipment in a second step. The measurements were performed in duplicate. The ash content was estimated by difference.

The morphology of the samples was studied with a Scanning Electron Microscope (FEG-SEM Hitachi S 4800) equipped with an EDX (Energy Dispersion of X-rays) instrument. The latter was used for semi-quantitative analysis and element mapping.

Calorific tests were carried out in a 6200 Isoperibolic Calorimeter (Parr) in order to determine the enthalpy of combustion of the raw biomass (Eucalyptus wood) and the biochar (CV). For that purpose, sample weights between 0.6 and 0.9 g were used and the variation of temperature while burning in an excess of oxygen was recorded. The measurements were performed with a resolution of 0.0001°C over a working range of 20 to 40°C.

The porous texture was characterised by N_2 adsorption-desorption at -196°C and by CO_2 adsorption at 0°C, using an automatic equipment (ASAP 2020, Micromeritics). First, the samples were outgassed at 110°C under secondary vacuum for at least 48h. The N_2 isotherms were used to estimate the apparent surface area, A_{BET} (m^2 g^{-1}), by applying the BET equation in the adequate range of relative pressures (p/p_0), and the total pore volume, V_T (cm^3 g^{-1}), at p/p_0 = 0.97. The p/p_0 range was chosen by plotting $V_{ads} \times (1 - p/p_0)$ as a function of p/p_0, V_{ads} being the STP adsorbed volume, and we took the range of values of p/p_0 for which $V_{ads} \times (1 - p/p_0)$ increased with p/p_0. The micropore volume, V_{DR} (cm^3 g^{-1}), was determined from the application of the Dubinin-Radushkevich (DR) equation to the N_2 adsorption, $V_{DR,N2}$, and to the CO_2 adsorption isotherms, $V_{DR,CO2}$ (Dubinin, 1989). The mesopore volume, V_{MESO} (cm^3 g^{-1}), was calculated as the difference between $V_{0.97}$ and $V_{DR,N2}$. The average pore size, L_0 (nm), was calculated using the following equation:

$$L_0(nm) = \frac{10.8}{E_0 - 11.4} \quad (2)$$

where E_0 (kJ mol^{-1}) is the characteristic adsorption energy derived from the application of the DR method to the N_2 adsorption isotherms (Stoeckli et al., 2000). The 2D NLDFT-HS method was applied to obtain the pore size distributions (PSD) from both the N_2 and CO_2 adsorption isotherms. Surface areas, S_{NLDFT} (m^2 g^{-1}), micropore volumes, $V_{\mu, NLDFT}$ (cm^3 g^{-1}), and total pore volumes, $V_{T, NLDFT}$ (cm^3 g^{-1}), were also obtained from the PSDs.

The textural information was supplemented by mercury porosimetry (Autopore IV, Micromeritics) to obtain macro and mesopore size distributions. The skeletal density of the solids was obtained by helium pycnometry (AccuPyc II 1340, Micromeritics), using samples previously degassed at 100°C under vacuum.

Given that the material yield is as important as the surface area, the total surface area, A_{TOTAL} (m^2 g^{-1}), can be used as a criterion for selecting materials for further testing (Acosta et al., 2016; Fierro et al., 2010). It reads:

$$A_{TOTAL} = \frac{A_{BET} \times Y}{100} \quad (3)$$

The pH at the point of zero charge, pH_{PZC}, which is the pH where the net charge of the surface is zero, was determined according to Carrott et al. (Carrott et al., 2001). Briefly, 15 mg of material was added to 15 mL of $NaNO_3$ solution (0.1 mol L^{-1}), bubbled with N_2 for 2 min, sealed and placed in a stirrer. The initial pH of the solution was recorded, and, after 48h of stirring, the suspension was filtered and the equilibrium pH was measured.

The amount of proton-binding groups was also measured. For that purpose, 0.1g of activated carbon was suspended in 50 mL of $NaNO_3$ solution (0.01 mol L^{-1}) as support electrolyte and was stirred overnight to equilibrate. The suspension was then titrated with NaOH (0.1 mol L^{-1}) under saturation with N_2 (Jagiello, 1994) using an automatic titrator (905 Titrando, Metrohm controlled by Tiamo® V2.2 software). The titration curves, pH vs volume, were transformed to proton-binding isotherms, Q vs pH, using the proton balance equation. Here, Q is equal to the total amount of protonated sites on the material. The relationship between the experimental proton-binding isotherms and pK_a values is given by an integral equation (Jagiello et al., 1995). The integration of this function over finite intervals, arbitrarily defined, gives the amount of sites whose pK_a values belong to these intervals. For the evaluation of the unknown distribution, $f(pK_a)$, the numerical SAIEUS-pK-Dist program was used.

175 *2.3 Paracetamol adsorption studies*

176 *2.3.1 Kinetic studies*

177 The materials were tested as paracetamol adsorbents in liquid phase. A paracetamol stock
178 solution of concentration 180 mg L^{-1} was prepared without adjusting the initial pH, which was
179 equal to 6. 98% pure paracetamol (Acros Organics) was used. The 2D and 3D structures of
180 paracetamol are shown in Figure SI 2.

181 For kinetic studies, 15 mg of carbon and 15 mL of paracetamol solution were mixed in a
182 glass flask that was introduced into a water bath at 30°C and stirred at 500 rpm in a 15-
183 position stirring plate (Mutistirrer 15, VELP Scientifica). After the desired contact time, an
184 aliquot was removed and the amount of paracetamol remaining in the solution was
185 determined by UV spectroscopy at 243 nm (Lambda 35 UV/VIS Spectrometer, Perkin
186 Elmer). All tests have been carried out in duplicate. The effect of the initial paracetamol
187 concentration, 10, 20 and 40 mg L^{-1} was studied.

188 The paracetamol uptake was calculated according to the following equation:

189 $$q_t = \frac{(C_0 - C_t)}{W} V \quad (4)$$

190 where q_t (mg g^{-1}) is the amount of paracetamol removed at time t, C_0 (mg L^{-1}) is the initial
191 concentration of paracetamol, C_t (mg L^{-1}) is the concentration of paracetamol at time t, V (L)
192 is the volume of the solution and W (g) is the weight of dry carbon.

193 *2.3.2 Kinetic modelling*

194 Two different kinetics models were applied to describe the experimental data. The first was
195 the pseudo-first order (PFO) kinetic model proposed by Lagergren (Lagergren, 1898),
196 mathematically represented by equation (5):

197 $$\frac{dq_t}{dt} = k_1(q_e - q_t) \quad (5)$$

where q_t and q_e are the adsorbed amounts (mg g^{-1}) at time t and at equilibrium, respectively, and k_1 (min^{-1}) is the kinetic rate constant of pseudo-first order.

The second kinetic model applied was the pseudo-second order (PSO) kinetic model proposed by Ho and McKay (Ho and McKay, 1999), and mathematically represented by equation (6):

$$\frac{dq_t}{dt} = k_2(q_e - q_t)^2 \quad (6)$$

where k_2 (g mg^{-1} min^{-1}) is the pseudo-second order rate constant.

The product $k_2 {q_e}^2$ represents the initial adsorption rate, h. The half-life time, t½, which is the time required for the adsorbent to uptake half of the adsorbate at equilibrium and which is often used as a measure of adsorption rate was also calculated. For PFO kinetic model, it is calculated according to equation (7) and, it is calculated according to equation (8) for the PSO:

$$t_{1/2} = \frac{\ln 2}{k_1} \quad (7)$$

$$t_{1/2} = \frac{1}{k_2\, q_e} \quad (8)$$

2.3.3 Equilibrium tests

Adsorption studies at equilibrium were carried out at 20, 30 and 40°C by varying the paracetamol concentration (5 – 180 mg L^{-1}) for the materials CV and CV15. After 5 days and 24h of stirring, respectively, to guarantee equilibrium, the sample suspensions were filtered and diluted if necessary. Then, the concentration of paracetamol remaining in solution at equilibrium (C_e) was determined, and the corresponding uptake (q_e) was calculated using equation (4). Experiments were done in duplicate.

The isotherms were modelled with the Langmuir, Freundlich and Sips equations (9), (10) and (11), respectively:

$$q_e = \frac{K_L\, q_m C_e}{1+K_L\, C_e} \quad (9)$$

where q_e and C_e have the same meaning as before, K_L (L mg^{-1}) is the Langmuir constant, and q_m (mg g^{-1}) is the monolayer adsorption capacity.

$$q_e = K_F\, (C_e)^{1/n} \quad (10)$$

where K_F (mg$^{1-1/n}$ L$^{1/n}$ g^{-1}) is the Freundlich constant and n (dimensionless) is the Freundlich exponent.

$$q_e = \frac{q_m\, (K_S C_e)^{1/n_S}}{1+\, (K_S C_e)^{1/n_S}} \quad (11)$$

where K_S (L mg^{-1}) is the Sips constant, and n_S (dimensionless) is the heterogeneity factor.

The BET liquid adsorption equilibrium model was also fitted to the experimental data, since this model considers the possibility of multilayer adsorption. The model is mathematically represented by equation (12).

$$q_e = \frac{q_m\, K_{BET} C_e}{(C_S - C_e)\left[1+(\, K_{BET}-1)\frac{C_e}{C_S}\right]} \quad (12)$$

where K_{BET} (L mg^{-1}) is the BET constant, and C_s (mg g^{-1}) is the saturation concentration of paracetamol in water.

2.3.4 Parameter estimation

All the parameters were estimated using as an objective function the sum of the square of errors, obtained through equation (13):

$$F_{OBJ} = \sum_{i=1}^{n_{dat}} \left(Y_{i,exp} - Y_{i,mod}\right)^2 \quad (13)$$

where F_{OBJ} is the objective function value, n_{dat} is the number of experimental points and $Y_{i,exp}$ and $Y_{i,mod}$ are respectively the experimental and predicted value for the experimental point i.

241 The method of Nelder and Mead was applied to such optimisation, using the mathematic
242 software Maple®.

243 **3. Results and discussion**

244 *3.1. Characterization of the carbon materials*

245 *3.1.1 Calorific value and elemental composition*

246 The average heat of combustion of CV (27.3 MJ kg^{-1}) was higher than that of wood (17.8
247 MJ kg^{-1}). These calorific values are consistent with what has been reported in the literature for
248 different species of Eucalyptus (Gaqa et al., 2014; Heidari et al., 2014; Khider and Elsaki,
249 2012; Kumar et al., 2010) and are slightly lower than for Eucalyptus-derived chars produced
250 by fast pyrolysis using a pilot-scale fluidised bed reactor (Heidari et al., 2014). These trends
251 have also been reported for other agroforestry tree crops (Fuwape, 1993; Khider and Elsaki,
252 2012) and for other types of biomass such as corn crop residues (Mullen et al., 2010). The
253 calorific value obtained here indicates that CV can be potentially used as fuel.

254 Table 1 presents the elemental analysis of the different materials studied. The carbon
255 content in the original sample (CV) was 81.8 wt. % and it slightly decreased after
256 carbonisation at 900°C to 80.6 wt. %. Activation with CO_2 further decreased the carbon
257 content due to evolution of volatiles and enrichment in ashes of the activated carbons. Thus,
258 the ash content of the CV sample was 4.4 wt. %, and increased up to 10.7 wt. % after
259 carbonisation at 900°C and even to 46.4 wt. % after CO_2 activation for 60 min. The hydrogen
260 and nitrogen contents were low, and there was no significant difference between the materials.

261 **Table 1.** Elemental composition (wt. %), yield *Y* (%) and pH_{PZC} of the materials.

Sample	C	H	N	O	S	Ash*	*Y* (%)	pH_{PZC}
CV	81.8	1.8	0.4	11.6	0.0	4.4	100	8.3
CV0	80.6	0.8	0.4	7.5	0.0	10.7	81.7	10.3

CV15	80.5	0.8	0.5	7.2	0.0	11.0	61.4	11.3
CV30	74.9	0.9	0.7	9.3	0.0	14.3	41.1	11.7
CV60	40.2	1.4	0.5	11.5	0.1	46.4	10.8	-

* Calculated as 100 – all other element weight fractions.

The SEM images in Figure 1a show that the wood structure was preserved after carbonisation and activation, and an increase in the ash content can be observed with activation, see Figure 1b. Thus, CV60 contained nearly 50 wt .% of ashes, clearly seen in the photo. A basic characterisation of this material was done just to illustrate trends, but no further paracetamol adsorption tests was performed on it. EDX analysis allowed to identifying and mapping inorganic components in the ashes, see Figure 1c. Among these, calcium was the major element identified ranging from 6 wt. % in CV to 30 wt. % in CV30. Mg, K, Fe and Al contents ranged between 2 wt. % and 6 wt. %, with no clear trend. Other elements such as Si, P, Na, Cu and Mn were identified but at lower percentages (<1 wt. %). These results are consistent with already reported ash composition of Eucalyptus wood (Girón et al., 2012; Khanna et al., 1994).

Figure 1

3.1.2 Textural properties

Figure 2a shows the N_2 adsorption/desorption isotherms of the materials. The original sample (CV) presents, according to the IUPAC classification, a type I isotherm with a marked knee in the region of low relative pressure and a slight slope at higher relative pressures (Thommes et al., 2015). This is characteristic of essentially microporous materials with a narrow micropore size distribution and an absence of significant mesoporosity, as also shown by the PSD (Figure 2d). The longer the activation time, the wider the knee and the higher the slope, indicating a widening of the micropore size distribution and the development of mesoporosity. The hysteresis loop appears and becomes more marked with the activation time, which is attributed to capillary condensation in the mesopores (Lin and Teng, 2002).

285 Figure 2

286 It is well known that following the activation step, which is a controlled gasification of the
287 carbon, part of the material is lost (called burn-off, BO (%) = 100 – *Y* (%). The extent of the
288 activation influences the morphology and the textural properties of the activated carbons (Al
289 Bahri et al., 2016). As shown in Table 1, the carbon yield decreased with the activation time:
290 from 81.7% for the reference material (CV0) to 10.8% after 60 minutes of exposure to CO_2.
291 Concerning the BET area (A_{BET}), see Figure 3, activation with CO_2 increased it from 392 to
292 845 m^2 g^{-1} from CV to CV30, respectively. CO_2 developed the pore texture over the entire
293 range of pore diameters, in particular the microporosity by opening closed pores as well as
294 widening existing ones, in agreement with previous studies (Rodríguez-Reinoso et al., 1995).

295 The pore texture parameters of all carbon materials are presented in Figure 3 and in Table
296 SI 4. By comparing CV to CV0, A_{BET} increased from 392 to 498 m^2 g^{-1}, due to the usual
297 volatile evolution when increasing the temperature from 700°C (typical Kon-Tiki charring
298 temperature) to 900°C. The tars produced during pyrolysis at 700°C could partially block the
299 micropores that would be opened at 900°C (Ibarra et al., 1991), as suggested by the values of
300 L_0 that did not change when increasing the pyrolysis temperature from 700 to 900°C (i.e.,
301 from CV to CV0, see Table SI 4). A_{BET} reached a maximum value of 845 m^2 g^{-1} after 30 min
302 of CO_2 activation but decreased by around 10% when the activation time was 60 min (Figure
303 3 and Table SI 4). Despite the fact that the ash-free fraction of CV60 may have a very high
304 surface area, this material also has a high ash content and ashes do not have a significant
305 surface area. Except for CV60, all the materials had higher $V_{DR,\ CO2}$ values than $V_{DR,\ N2}$,
306 suggesting that a significant part of the microporosity was not accessible to N_2 at the
307 equilibrium times given for this analysis. This also means that, to give an accurate overview
308 of the textural properties of the materials, both N_2 and CO_2 adsorption isotherms must be
309 taken into account, as this has been shown in Figure 2c. Therefore, $V_{DR,\ N2}$, $V_{DR,\ CO2}$ and $V_{0.97}$

are given for comparison with textural data reported in the open literature, but $V_{\mu, NLDFT}$ and $V_{T, NLDFT}$ give a more precise indication of the microporosity and total porosity, respectively (see Figure SI 3 and Table SI 4).

Figure 3 shows the evolution of the A_{BET}, A_{TOTAL}, S_{NLDFT}, the total and micropore volume and the average pore size with the burn-off (BO, wt. %). While A_{BET} and S_{NLDFT} showed a marked increase from 392 to 845 $m^2 g^{-1}$ and from 600 to 1000 $m^2 g^{-1}$ at 30 min of activation (58.9 % BO), respectively, A_{TOTAL} only slightly increased from 392 to 415 $m^2 g^{-1}$ at 15 min of activation (39.6% BO) and markedly decreased afterwards. The microporosity fraction decreased with the increase in the burn-off. Based on previous studies (Acosta et al., 2016; Basta et al., 2009; Selmi et al., 2018), we selected CV15 for further paracetamol adsorption studies because a good compromise between A_{BET} and Y was reached.

Figure 3

Figure 2d shows that CV presented a bimodal PSD, with a narrow peak centred at 0.4 nm and some pores with a diameter of 0.75 nm. The PSD widened with the activation time up to CV30 at the same time as the pores narrower than 1 nm increased. CV60 showed a continuous PSD with an enlargement of the pore size. Besides, mercury porosimetry suggests a higher volume of mesopores in the activated carbons (Figure 4).

Figure 4

Figure 4 shows the PSD in the mesopore (2-50 nm) and macropore (> 50 nm) ranges. However, the equipment used for mercury intrusion, with a maximum intrusion pressure of 414 MPa, only allows access to pores with diameters greater than 3.6 nm. CV and CV0 showed very similar PSDs, but the amount of pores narrower than 100 nm decreased compared to those of larger diameter, in agreement with the higher ash content of ACs

produced at longer activation times. The bulk density of the materials calculated at a mercury intrusion pressure of 0.0036 MPa decreased from 0.21 g cm^{-3} for CV to 0.16 g cm^{-3} for CV60, which suggests the increase of porosity of the materials with the activation time, not only in the micropore range already evidenced by N_2 + CO_2 adsorption, but also in the mesopore and macropore ranges.

3.1.3 Surface chemistry

With respect to surface chemistry, the values of pH_{PZC} shown in Table 1 suggest that CV and derived ACs have a basic nature. Although the ash contents were only quantified for raw eucalyptus biomass and CV, a simple visual analysis of Figure 1b and the estimation presented from the elemental analysis revealed that ashes became noticeable as the activation time increased, and were evident in CV60. Then, a basic nature of the ACs was expected and it should be greatly influenced by the ash content.

A more detailed analysis was performed on samples CV and CV15 to study the modification of surface functionalities with the activation process. Figure 5 shows the results of the potentiometric titration of these materials. Activation increased the density of functional groups from 0.63 to 1.04 mmol g^{-1} (see Table 2). The number of peaks, representing different types of functional groups, was 4 and 5 for CV and CV15, respectively. The pK_a distributions showed the predominance of strongly basic species such as lactol- or hydroxyl-containing functional groups with $pK_a > 8$ (Seredych et al., 2015). The basicity of CV and CV15 materials was confirmed by the high value of pH_{PZC}, around 8 and 11, respectively (see again Table 1).

Figure 5

Table 2. Results of potentiometric titration measurements: peak position and number of types of functional groups (mmol/g, in brackets); the pH_{PZC} is also recalled.

Samples	pK_a 3-5	pK_a 5-7	pK_a 7-8	pK_a 8-10	pK_a 10-12	All (mmol g^{-1})	pH_{PZC}
CV	3.79 (0.02)	5.35 (0.05)	-	8.16 (0.09)	11.33 (0.46)	0.63	8.3
CV15	4.41 (0.08)	6.21 (0.04)	7.78 (0.19)	9.63 (0.22)	10.91 (0.51)	1.04	11.3

This analysis is relevant given that changes in the surface chemistry of activated carbons can also affect the adsorption process of pollutants by dissociation of functional groups on the adsorbent surface (Ruiz et al., 2010).

3.2 Removal of paracetamol in the liquid phase

3.2.1 Paracetamol adsorption kinetics

Figure 6 shows the kinetics of paracetamol adsorption at 30°C on CV, CV0, CV15 and CV30 for initial paracetamol concentrations of 10, 20 and 40 mg L^{-1}. While CV took almost 3 days to equilibrate, CV15 and CV30 reached equilibrium in 1h at C_0 = 10 mg L^{-1} and 5 h at C_0 = 40 mg L^{-1}. CV0 reached equilibrium in about 5h at C_0 = 10 mg L^{-1} and 12h at C_0 = 40 mg L^{-1}. For the three ACs (CV0, CV15 and CV30), the removal of paracetamol at equilibrium was complete for the three concentrations tested. The experimental kinetic data were best fitted by the pseudo-second order kinetic model.

Figure 6

Table SI 5 shows the kinetic parameters derived from the application of PFO and PSO models, and the corresponding determination coefficients R^2. For the three concentrations of paracetamol tested, a longer activation time had a positive effect on the initial (h) and global (k_1 and k_2) adsorption rates, and reduction of the adsorption half-time ($t_{1/2}$), i.e., the time required to reach half of the paracetamol uptake at equilibrium. For example, $t_{1/2}$ at the highest initial concentration (40 mg L^{-1}) for CV15 and CV30 was 6 minutes while it was 282

377 min for CV. Then, it can be concluded that the adsorption process of paracetamol is faster
378 with activation. Given the dimensions of the paracetamol molecule (0.46 nm and 0.66 nm for
379 monomer and dimer, respectively), micropores are known to be the active sites with the
380 highest adsorption potential for its removal from the liquid phase (Mestre et al., 2009). Thus,
381 a higher volume of micro- and mesopores and a wider micropore size distribution should
382 allow a faster diffusion of paracetamol molecules in the materials.

383 The initial concentration of paracetamol did not show a marked effect on the PFO constant.
384 However, the parameter k_2 decreased with the increase in C_0, in agreement with previous
385 studies of adsorption of diuron (Al Bahri et al., 2016) or ibuprofen (Mestre et al., 2007).

386 Regarding the removal efficiency, there was no significant difference between the ACs for
387 all the concentrations tested (removal between 96 and 99%). For low initial concentrations of
388 paracetamol (10 mg L^{-1}), the CV removed as much paracetamol as ACs at equilibrium, but its
389 performance decreased with the increase in C_0. This is an interesting result, given that this
390 type of pollutant is present at low concentrations in the environment. Since the production of
391 CV is an easy and reproducible process, which does not require any exceptional equipment, it
392 is a promising material to continue exploring in difficult economic contexts.

393 *3.2.2 Paracetamol equilibrium adsorption studies*

394 The paracetamol adsorption isotherms displayed in Figure 7 suggest that the adsorption
395 mechanisms of the original carbon (CV) and the activated carbon CV15 were the same, as
396 both were type II (Brunauer et al., 1940). The isotherm obtained for CV15 has two defined
397 regions: in the first, a steep initial rise that approaches a plateau is observed and, in the second
398 region, an upward curvature is recorded for higher equilibrium paracetamol concentrations.
399 The former phenomenon is related to the formation of a complete monolayer, while the latter
400 is explained by multilayer or aggregate formation at the interface at high coverage (Girods et

al., 2009). The formation of multilayers could be related to the characteristics of the adsorbent surface and to the pH of the medium, which could affect the interactions between the solvent, the adsorbate and the adsorbent (Al Bahri et al., 2016). This type of isotherm has also been reported by Terzyk and Rychlicki (Terzyk and Rychlicki, 2000) for some chemically ACs when removing paracetamol at similar concentrations, but this is not the usual behaviour reported in the literature concerning paracetamol adsorption. However, it has been also observed for other pollutants such as phenol (Girods et al., 2009), cationic dyes (Cotoruelo et al., 2011) and diuron (Al Bahri et al., 2016). Figure 7a shows a higher paracetamol uptake at 20°C compared to that determined at 30°C, which could be related to the experimental uncertainty (the error bars of the two temperatures indeed overlap), as well as to small uptake differences between these two fairly close temperatures.

Figure 7

Langmuir, Freundlich and Sips models were fitted to the data corresponding to CV and CV15 samples (see Table SI 6 and Figures SI 10 and SI 11). In addition, the Langmuir and Freundlich models were applied to the monolayer region only (see Table SI 7 and Figure SI 8). This approach gave results different from those obtained when applied to the entire range of equilibrium experimental data. Since the isotherms were type II, multilayer adsorption may be better described by applying the BET equation in the liquid phase (Brunauer et al., 1938). Table SI 9 summarises the parameters derived from this model.

The monolayer adsorption capacities q_m derived from the application of the BET model were equal to the values obtained when the Langmuir model was applied to the monolayer region. The values obtained were in the range of 14.4 to 14.9 mg g^{-1} and 88.1 to 98.2 mg g^{-1} for CV and CV15, respectively. In addition, the ratios of the K_{BET} and C_s parameters were very close to the values of K_L of the monolayer region. This proximity of the parameters

means that at low concentration, the two models converge towards a very similar value of Henry's constant.

As far as the effect of temperature is concerned, there is no clear trend. The calculated parameters, such as the equilibrium constant K_L and the monolayer capacity q_m of the Langmuir equation, do not change gradually with increasing temperature. Contrasting results have been reported in literature. Consistent with our study, some authors ((Baccar et al., 2012) and (Mestre et al., 2007)) did not notice any effect of temperature on the removal of pharmaceutical products, among them ibuprofen and diclofenac. More specifically on paracetamol, while García-Mateos et al. (García-Mateos et al., 2015) reported an exothermic nature of the adsorption process (i.e., the uptake decreased with temperature), others ((Terzyk and Rychlicki, 2000) and (Cotoruelo et al., 2011)) observed an endothermic behaviour (i.e., the uptake increased with temperature). Moreover, Villaescusa et al. (Villaescusa et al., 2011) reported similar sorption capacity when the temperature was maintained in the range of 5–20°C, but a slight increase in sorption was observed when the temperature was increased to 25–30°C.

3.3 Comparison with data from the literature

Figure 8 collects information related to paracetamol removal with different types of activated carbons and modified carbons reported in the literature (Cabrita et al., 2010; Cotoruelo et al., 2011; Galhetas et al., 2014a, 2014b; García-Mateos et al., 2015; Mestre et al., 2015) and in the present study. Comparison with the literature is sometimes difficult because experimental variables chosen for materials synthesis and removal assays differ considerably from one study to another. For instance, the paracetamol concentrations tested here are significantly lower, but more realistic, than those used in other articles, whereas they have a very high influence on the adsorption capacities obtained in this work.

Figure 8

There is a trend (R^2 = 0.78) that suggests that the higher the surface area, the higher the maximum paracetamol removal capacity (q_m). As mentioned in many articles, surface chemistry also influences the removal capacity, and different activation processes and/or heteroatom doping can introduce changes in the surface functionalities of the ACs. Hence, the surface functional groups and the net surface charge might explain the variability remaining unexplained in the material performance.

4. Conclusion

Four microporous activated carbons were obtained from a biochar precursor, called CV, produced with Eucalyptus pruning residues charred in a simple and low-cost device, a Kon-Tiki kiln. Additional CO_2 activation significantly enhanced the specific surface area, the total pore volume and the micropore volume.

The equilibrium paracetamol (PC) adsorption was reached at 5h for the activated carbons and at 3 days for their precursor at the highest initial paracetamol concentration tested, and a pseudo-second order model suitably fitted the experimental data. The textural characterisation suggested an opening and widening of micropores and a development of mesopores with CO_2 activation, which favoured the diffusion of paracetamol molecules in the material.

At low concentrations, which are the most realistic for this type of contaminants, CV had a very high removal efficiency, similar to those of the activated carbons tested (> 95 %). A simple adjustment (i.e., an increase) in the solid / liquid ratio might be enough to reduce the time for the efficient treatment of water in vulnerable communities with such inexpensive carbon material.

Concerning paracetamol uptake at equilibrium, CV and CV15 showed a favourable adsorption and the corresponding isotherms suggested the formation of paracetamol multilayers. The equilibrium adsorption capacities of CV15, whether for monolayer or multilayer adsorption, were about 5 times higher than for CV. This has been attributed to the more developed textural properties of CV15.

Acknowledgements

Amalia Bursztyn gratefully acknowledges CONICET for the PhD scholarship and Martiniano Picicco who helped with the carbonisation. The IJL members gratefully acknowledge the financial support of TALiSMAN project, funded by FEDER (2019-000214).

References

Acosta, R., Fierro, V., Martinez de Yuso, A., Nabarlatz, D., Celzard, A., 2016. Tetracycline adsorption onto activated carbons produced by KOH activation of tyre pyrolysis char. Chemosphere 149, 168–176. https://doi.org/10.1016/j.chemosphere.2016.01.093

Al Bahri, M., Calvo, L., Gilarranz, M.A., Rodriguez, J.J., 2016. Diuron Multilayer Adsorption on Activated Carbon from CO2Activation of Grape Seeds. Chem. Eng. Commun. 203, 103–113. https://doi.org/10.1080/00986445.2014.934447

Baccar, R., Sarrà, M., Bouzid, J., Feki, M., Blánquez, P., 2012. Removal of pharmaceutical compounds by activated carbon prepared from agricultural by-product. Chem. Eng. J. 211–212, 310–317. https://doi.org/10.1016/j.cej.2012.09.099

Basta, A.H., Fierro, V., El-Saied, H., Celzard, A., 2009. 2-Steps KOH activation of rice straw: An efficient method for preparing high-performance activated carbons. Bioresour. Technol. 100, 3941–3947. https://doi.org/10.1016/j.biortech.2009.02.028

Boudrahem, N., Delpeux-Ouldriane, S., Khenniche, L., Boudrahem, F., Aissani-Benissad, F., Gineys, M., 2017. Single and mixture adsorption of clofibric acid, tetracycline and paracetamol onto Activated carbon developed from cotton cloth residue. Process Saf. Environ. Prot. 111, 544–559. https://doi.org/10.1016/j.psep.2017.08.025

Bound, J.P., Voulvoulis, N., 2006. Predicted and measured concentrations for selected pharmaceuticals in UK rivers: Implications for risk assessment. Water Res. 40, 2885–2892. https://doi.org/10.1016/j.watres.2006.05.036

Brunauer, S., Deming, L.S., Deming, W.E., Teller, E., 1940. On a Theory of the van der Waals Adsorption of Gases. J. Am. Chem. Soc. 62, 1723–1732. https://doi.org/10.1021/ja01864a025

506 Brunauer, S., Emmett, P.H., Teller, E., 1938. Adsorption of Gases in Multimolecular Layers.
507 J. Am. Chem. Soc. 60, 309–319. https://doi.org/10.1021/ja01269a023

508 Cabrita, I., Ruiz, B., Mestre, A.S., Fonseca, I.M., Carvalho, A.P., Ania, C.O., 2010. Removal
509 of an Analgesic Using Activated Carbons Prepared From. Chem. Eng. J. 163, 1–28.
510 https://doi.org/10.1016/j.cej.2010.07.058

511 Carrott, P.J.M., Nabais, J.M.V., Ribeiro Carrott, M.M.L., Menéndez, J.A., 2001. Thermal
512 treatments of activated carbon fibres using a microwave furnace. Microporous
513 Mesoporous Mater. 47, 243–252. https://doi.org/10.1016/S1387-1811(01)00384-5

514 Cornelissen, G., Pandit, N.R., Taylor, P., Pandit, B.H., Sparrevik, M., Schmidt, H.P., 2016.
515 Emissions and char quality of flame-curtain "Kon Tiki" kilns for farmer-scale
516 charcoal/biochar production. PLoS One 11, 1–16.
517 https://doi.org/10.1371/journal.pone.0154617

518 Correia, B., Freitas, R., Figueira, E., Soares, A.M.V.M., Nunes, B., 2016. Oxidative effects of
519 the pharmaceutical drug paracetamol on the edible clam Ruditapes philippinarum under
520 different salinities. Comp. Biochem. Physiol. Part - C Toxicol. Pharmacol. 179, 116–
521 124. https://doi.org/10.1016/j.cbpc.2015.09.006

522 Cotoruelo, L.M., Marqués, M.D., Leiva, A., Rodríguez-Mirasol, J., Cordero, T., 2011.
523 Adsorption of oxygen-containing aromatics used in petrochemical, pharmaceutical and
524 food industries by means of lignin based active carbons. Adsorption 17, 539–550.
525 https://doi.org/10.1007/s10450-010-9319-x

526 Daughton, C.G., Ternes, T.A., 1999. Pharmaceuticals and Personal Care Products in the
527 Environment : Agents of Subtle Change? Environ. Health Perspect. 107, 907–938.

528 Dordio, A. V., Estêvão Candeias, A.J., Pinto, A.P., Teixeira da Costa, C., Palace Carvalho,

A.J., 2009. Preliminary media screening for application in the removal of clofibric acid, carbamazepine and ibuprofen by SSF-constructed wetlands. Ecol. Eng. 35, 290–302. https://doi.org/10.1016/j.ecoleng.2008.02.014

Dubinin, M.M., 1989. Fundamentals of the theory of adsorption in micropores of carbon adsorbents: Characteristics of their adsorption properties and microporous structures. Carbon N. Y. 27, 457–467. https://doi.org/10.1016/0008-6223(89)90078-X

Fierro, V., Muñiz, G., Basta, A.H., El-Saied, H., Celzard, A., 2010. Rice straw as precursor of activated carbons: Activation with ortho-phosphoric acid. J. Hazard. Mater. 181, 27–34. https://doi.org/10.1016/j.jhazmat.2010.04.062

Fierro, V., Torné-Fernández, V., Celzard, A., 2006. Kraft lignin as a precursor for microporous activated carbons prepared by impregnation with ortho-phosphoric acid: Synthesis and textural characterisation. Microporous Mesoporous Mater. 92, 243–250. https://doi.org/10.1016/j.micromeso.2006.01.013

Fuwape, J.A., 1993. Charcoal and fuel value of agroforestry tree crops. Agrofor. Syst. 22, 175–179. https://doi.org/10.1007/BF00705232

Galhetas, M., Mestre, A.S., Pinto, M.L., Gulyurtlu, I., Lopes, H., Carvalho, A.P., 2014a. Carbon-based materials prepared from pine gasification residues for acetaminophen adsorption. Chem. Eng. J. 240, 344–351. https://doi.org/10.1016/j.cej.2013.11.067

Galhetas, M., Mestre, A.S., Pinto, M.L., Gulyurtlu, I., Lopes, H., Carvalho, A.P., 2014b. Chars from gasification of coal and pine activated with K2CO3: Acetaminophen and caffeine adsorption from aqueous solutions. J. Colloid Interface Sci. 433, 94–103. https://doi.org/10.1016/j.jcis.2014.06.043

Gaqa, S., Mamphweli, S., Katwire, D., Meyer, E., 2014. The Properties and Suitability of

552 Various Biomass/Coal Blends for Co-Gasification Purposes. J. Sustain. Bioenergy Syst.
553 04, 175–182. https://doi.org/10.4236/jsbs.2014.43016

554 García-Mateos, F.J., Ruiz-Rosas, R., Marqués, M.D., Cotoruelo, L.M., Rodríguez-Mirasol, J.,
555 Cordero, T., 2015. Removal of paracetamol on biomass-derived activated carbon:
556 Modeling the fixed bed breakthrough curves using batch adsorption experiments. Chem.
557 Eng. J. 279, 18–30. https://doi.org/10.1016/j.cej.2015.04.144

558 Girods, P., Dufour, A., Fierro, V., Rogaume, Y., Rogaume, C., Zoulalian, A., Celzard, A.,
559 2009. Activated carbons prepared from wood particleboard wastes: Characterisation and
560 phenol adsorption capacities. J. Hazard. Mater. 166, 491–501.
561 https://doi.org/10.1016/j.jhazmat.2008.11.047

562 Girón, R.P., Suárez-Ruiz, I., Ruiz, B., Fuente, E., Gil, R.R., 2012. Fly ash from the
563 combustion of forest biomass (Eucalyptus globulus bark): Composition and
564 physicochemical properties. Energy and Fuels 26, 1540–1556.
565 https://doi.org/10.1021/ef201503u

566 Gros, M., Petrović, M., Barceló, D., 2006. Development of a multi-residue analytical
567 methodology based on liquid chromatography-tandem mass spectrometry (LC-MS/MS)
568 for screening and trace level determination of pharmaceuticals in surface and
569 wastewaters. Talanta 70, 678–690. https://doi.org/10.1016/j.talanta.2006.05.024

570 Heidari, A., Stahl, R., Younesi, H., Rashidi, A., Troeger, N., Ghoreyshi, A.A., 2014. Effect of
571 process conditions on product yield and composition of fast pyrolysis of Eucalyptus
572 grandis in fluidized bed reactor. J. Ind. Eng. Chem. 20, 2594–2602.
573 https://doi.org/10.1016/j.jiec.2013.10.046

574 Ho, Y.S., McKay, G., 1999. Pseudo-second order model for sorption processes. Process

575 Biochem. 34, 451–465.

576 Ibarra, J. V., Moliner, R., Palacios, J.M., 1991. Catalytic effects of zinc chloride in the
577 pyrolysis of Spanish high sulphur coals. Fuel 70, 727–732.

578 Jagiello, J., 1994. Stable Numerical Solution of the Adsorption Integral Equation Using
579 Splines. Langmuir 10, 2778–2785. https://doi.org/10.1021/la00020a045

580 Jagiello, J., Badosz, T., Putyera, K., Schwarz, J., 1995. Determination of Proton Affinity
581 Distributions for Chemical Systems in Aqueous Environments Using a Stable Numerical
582 Solution of the Adsorption Integral Equation. J. Colloid Interface Sci. 172, 341–346.
583 https://doi.org/https://doi.org/10.1006/jcis.1995.1262

584 Khanna, P.K., Raison, R.J., Falkiner, R.A., 1994. Chemical properties of ash derived from
585 Eucalyptus litter and its effects on forest soils. For. Ecol. Manage. 66, 107–125.
586 https://doi.org/10.1016/0378-1127(94)90151-1

587 Khider, T.O., Elsaki, O.T., 2012. Heat Value of Four Hardwood Species from. J. For. Prod.
588 Ind. 1, 5–9.

589 Kolpin, D.W., Furlong, E.T., Meyer, M.T., Thurman, E.M., Zaugg, S.D., Barber, L.B.,
590 Buxton, H.T., 2002. Pharmaceuticals, hormones, and other organic wastewater
591 contaminants in U.S. streams, 1999-2000: A national reconnaissance. Environ. Sci.
592 Technol. 36, 1202–1211. https://doi.org/10.1021/es011055j

593 Kumar, R., Pandey, K.K., Chandrashekar, N., Mohan, S., 2010. Effect of tree-age on calorific
594 value and other fuel properties of Eucalyptus hybrid. J. For. Res. 21, 514–516.
595 https://doi.org/10.1007/s11676-010-0108-x

596 Lagergren, S., 1898. Zur theorie der sogenannten adsorption gelöster stoffe, Kungliga

Svenska Vetenskapsakademiens. Handlingar 24, 1–39.

Lin, Y.R., Teng, H., 2002. Mesoporous carbons from waste tire char and their application in wastewater discoloration. Microporous Mesoporous Mater. 54, 167–174. https://doi.org/10.1016/S1387-1811(02)00380-3

Lladó, J., Lao-Luque, C., Ruiz, B., Fuente, E., Solé-Sardans, M., Dorado, A.D., 2015. Role of activated carbon properties in atrazine and paracetamol adsorption equilibrium and kinetics. Process Saf. Environ. Prot. 95, 51–59. https://doi.org/10.1016/j.psep.2015.02.013

Marques, S.C.R., Marcuzzo, J.M., Baldan, M.R., Mestre, A.S., Carvalho, A.P., 2017. Pharmaceuticals removal by activated carbons: Role of morphology on cyclic thermal regeneration. Chem. Eng. J. 321, 233–244. https://doi.org/10.1016/j.cej.2017.03.101

Mestre, A.S., Bexiga, A.S., Proença, M., Andrade, M., Pinto, M.L., Matos, I., Fonseca, I.M., Carvalho, A.P., 2011. Activated carbons from sisal waste by chemical activation with K 2CO 3: Kinetics of paracetamol and ibuprofen removal from aqueous solution. Bioresour. Technol. 102, 8253–8260. https://doi.org/10.1016/j.biortech.2011.06.024

Mestre, A.S., Pires, J., Nogueira, J.M.F., Carvalho, A.P., 2007. Activated carbons for the adsorption of ibuprofen. Carbon N. Y. 45, 1979–1988. https://doi.org/10.1016/j.carbon.2007.06.005

Mestre, A.S., Pires, J., Nogueira, J.M.F., Parra, J.B., Carvalho, A.P., Ania, C.O., 2009. Waste-derived activated carbons for removal of ibuprofen from solution: Role of surface chemistry and pore structure. Bioresour. Technol. 100, 1720–1726. https://doi.org/10.1016/j.biortech.2008.09.039

Mestre, A.S., Tyszko, E., Andrade, M.A., Galhetas, M., Freire, C., Carvalho, A.P., 2015.

620 Sustainable activated carbons prepared from a sucrose-derived hydrochar: Remarkable
621 adsorbents for pharmaceutical compounds. RSC Adv. 5, 19696–19707.
622 https://doi.org/10.1039/c4ra14495c

623 Mullen, C.A., Boateng, A.A., Goldberg, N.M., Lima, I.M., Laird, D.A., Hicks, K.B., 2010.
624 Bio-oil and bio-char production from corn cobs and stover by fast pyrolysis. Biomass
625 and Bioenergy 34, 67–74. https://doi.org/10.1016/j.biombioe.2009.09.012

626 Pandit, N.R., Mulder, J., Hale, S.E., Schmidt, H.P., Cornelissen, G., 2017. Biochar from "Kon
627 Tiki" flame curtain and other kilns: Effects of nutrient enrichment and kiln type on crop
628 yield and soil chemistry. PLoS One 12, 1–12.
629 https://doi.org/10.1371/journal.pone.0176378

630 Rodríguez-Reinoso, F., Molina-Sabio, M., González, M.T., 1995. The use of steam and CO2
631 as activating agents in the preparation of activated carbons. Carbon N. Y. 33, 15–23.
632 https://doi.org/10.1016/0008-6223(94)00100-E

633 Ruiz, B., Cabrita, I., Mestre, A.S., Parra, J.B., Pires, J., Carvalho, A.P., Ania, C.O., 2010.
634 Surface heterogeneity effects of activated carbons on the kinetics of paracetamol removal
635 from aqueous solution. Appl. Surf. Sci. 256, 5171–5175.
636 https://doi.org/10.1016/j.apsusc.2009.12.086

637 Schaefer, S., Fierro, V., Izquierdo, M.T., Celzard, A., 2016. Assessment of hydrogen storage
638 in activated carbons produced from hydrothermally treated organic materials. Int. J.
639 Hydrogen Energy 41, 12146–12156. https://doi.org/10.1016/j.ijhydene.2016.05.086

640 Schmidt, H.-P., Taylor, P., 2014. Kon-Tiki - the democratization of biochar production
641 [WWW Document]. Biochar J.

642 Selmi, T., Sanchez-Sanchez, A., Gadonneix, P., Jagiello, J., Seffen, M., Sammouda, H.,

643 Celzard, A., Fierro, V., 2018. Tetracycline removal with activated carbons produced by
644 hydrothermal carbonisation of Agave americana fibres and mimosa tannin. Ind. Crops
645 Prod. 115, 146–157. https://doi.org/10.1016/j.indcrop.2018.02.005

646 Seredych, M., Biggs, M.J., Bandosz, T.J., 2015. Oxygen reduction on chemically
647 heterogeneous iron-containing nanoporous carbon: The effects of specific surface
648 functionalities. Microporous Mesoporous Mater. 221, 137–149.
649 https://doi.org/10.1016/j.micromeso.2015.09.032

650 Spessato, L., Cazetta, A.L., Melo, S., Pezoti, O., Tami, J., Ronix, A., Fonseca, J.M., Martins,
651 A.F., Silva, T.L., Almeida, V.C., 2020. Synthesis of superparamagnetic activated carbon
652 for paracetamol removal from aqueous solution. J. Mol. Liq. 300.
653 https://doi.org/10.1016/j.molliq.2019.112282

654 Stoeckli, F., Guillot, A., Hugi-Cleary, D., Slasli, A.M., 2000. Pore size distributions of active
655 carbons assessed by different techniques. Carbon N. Y. 38, 938–941.
656 https://doi.org/10.1016/s0008-6223(00)00057-9

657 Szczurek, A., Amaral-Labat, G., Fierro, V., Pizzi, A., Celzard, A., 2014. Chemical activation
658 of tannin-based hydrogels by soaking in KOH and NaOH solutions. Microporous
659 Mesoporous Mater. 196, 8–17. https://doi.org/10.1016/j.micromeso.2014.04.051

660 Terzyk, A.P., 2001. The influence of activated carbon surface chemical composition on the
661 adsorption of acetaminophen (paracetamol) in vitro. Part II. TG, FTIR, and XPS analysis
662 of carbons and the temperature dependence of adsorption kinetics at the neutral pH.
663 Colloids Surfaces A Physicochem. Eng. Asp. 177, 23–45. https://doi.org/10.1016/S0927-
664 7757(00)00594-X

665 Terzyk, A.P., Rychlicki, G., 2000. The influence of activated carbon surface chemical

composition on the adsorption of acetaminophen (paracetamol) in vitro: The temperature dependence of adsorption at the neutral pH. Colloids Surfaces A Physicochem. Eng. Asp. 163, 135–150. https://doi.org/10.1016/S0927-7757(99)00298-8

Terzyk, A.P., Rychlicki, G., Biniak, S., Łukaszewicz, J.P., 2003. New correlations between the composition of the surface layer of carbon and its physicochemical properties exposed while paracetamol is adsorbed at different temperatures and pH. J. Colloid Interface Sci. 257, 13–30. https://doi.org/10.1016/S0021-9797(02)00032-2

Thommes, M., Kaneko, K., Neimark, A. V., Olivier, J.P., Rodriguez-Reinoso, F., Rouquerol, J., Sing, K.S.W., 2015. Physisorption of gases, with special reference to the evaluation of surface area and pore size distribution (IUPAC Technical Report). Pure Appl. Chem. 87, 1051–1069. https://doi.org/10.1515/pac-2014-1117

Villaescusa, I., Fiol, N., Poch, J., Bianchi, A., Bazzicalupi, C., 2011. Mechanism of paracetamol removal by vegetable wastes: The contribution of Π-Π interactions, hydrogen bonding and hydrophobic effect. Desalination 270, 135–142. https://doi.org/10.1016/j.desal.2010.11.037

WHO, 2004. Guidelines for Drinking-water Quality, 3rd ed. WHO, Geneva.

Wiegel, S., Aulinger, A., Brockmeyer, R., Harms, H., Löffler, J., Reincke, H., Schmidt, R., Stachel, B., Von Tümpling, W., Wanke, A., 2004. Pharmaceuticals in the river Elbe and its tributaries. Chemosphere 57, 107–126. https://doi.org/10.1016/j.chemosphere.2004.05.017

Wu, S., Zhang, L., Chen, J., 2012. Paracetamol in the environment and its degradation by microorganisms. Appl. Microbiol. Biotechnol. 96, 875–884. https://doi.org/10.1007/s00253-012-4414-4

689 Zhang, T., Walawender, W.P., Fan, L.T., Fan, M., Daugaard, D., Brown, R.C., 2004.
690 Preparation of activated carbon from forest and agricultural residues through CO2
691 activation. Chem. Eng. J. 105, 53–59. https://doi.org/10.1016/j.cej.2004.06.011

692

693 **Captions of the Figures**

694 **Figure 1.** (a) SEM images of CV (500 ×, left) and CV30 (200 ×, right); (b) Photos of the
695 samples showing the increase in ash content with activation time; (c) Elemental mapping by
696 SEM-EDX of samples CV, CV0 and CV30.

697 **Figure 2.** Adsorption-desorption isotherms of (a) N_2 at -196°C and (b) CO_2 at 0°C; (c) fits of
698 the isotherms by the NLDFT for CV30; and (d) corresponding pore size distributions.

699 **Figure 3.** Changes of pore texture parameters as function of the burn-off: (a) surface areas
700 A_{BET}, A_{TOTAL}, and S_{NLDFT}; and (b) pore volumes (total and micropore) and average pore sizes.

701 **Figure 4**. Pore size distribution in the ranges of mesopores and macropores obtained by
702 mercury intrusion: (a) differential; and (b) cumulative Hg intrusion volumes.

703 **Figure 5.** Distribution of functional groups as a function of pK_a, for CV (blue) and CV15
704 (light brown) samples.

705 **Figure 6.** Fits of the PFO and PSO models to the experimental data of paracetamol adsorption
706 kinetics on CV, CV0, CV15 and CV30 at 30°C, with three different paracetamol initial
707 concentrations (10, 20 and 40 mg L^{-1}).

708 **Figure 7**. Experimental paracetamol adsorption isotherms at 20°C (red), 30°C (blue) and
709 40°C (green) for: (a) CV; and (b) CV15 samples. The symbols correspond to experimental
710 data whereas the lines represent the fits using the BET isotherm model.

711 **Figure 8.** Maximum paracetamol adsorption capacities of activated carbons (obtained in
712 similar experimental conditions) as a function of their BET surface area (1- Mestre et al,
713 2015; 2- Galhetas et al, 2014a; 3- Galhetas et al, 2014b; 4- Cotoruelo et al, 2011; 5- Cabrita et
714 al, 2010; 6- Spessato et al., 2020; 7- Lladó et al., 2015 and 8- Marques et al., 2017).

715

716

Paracetamol removal by Kon-Tiki kiln-derived biochar and activated carbons

Bursztyn Fuentes et al.

Figure 1

(a)

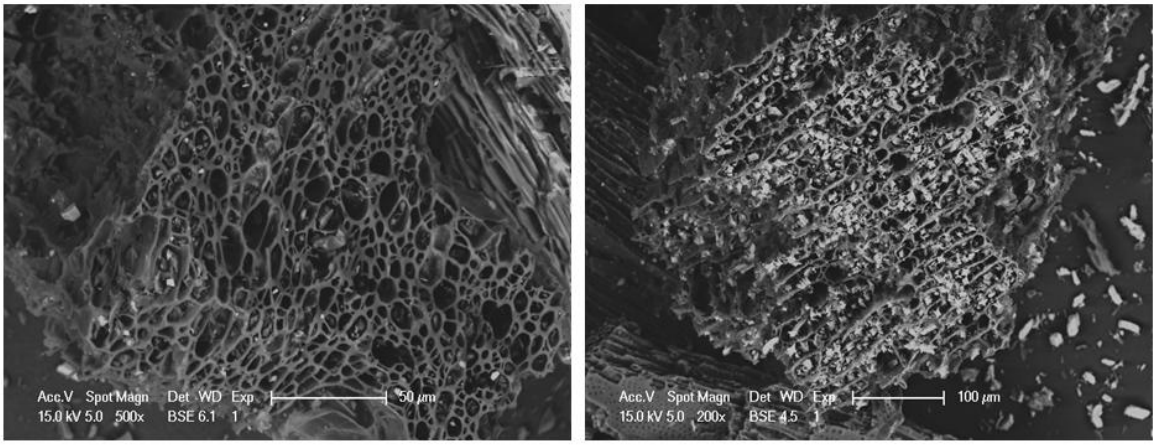

(b)

(c)

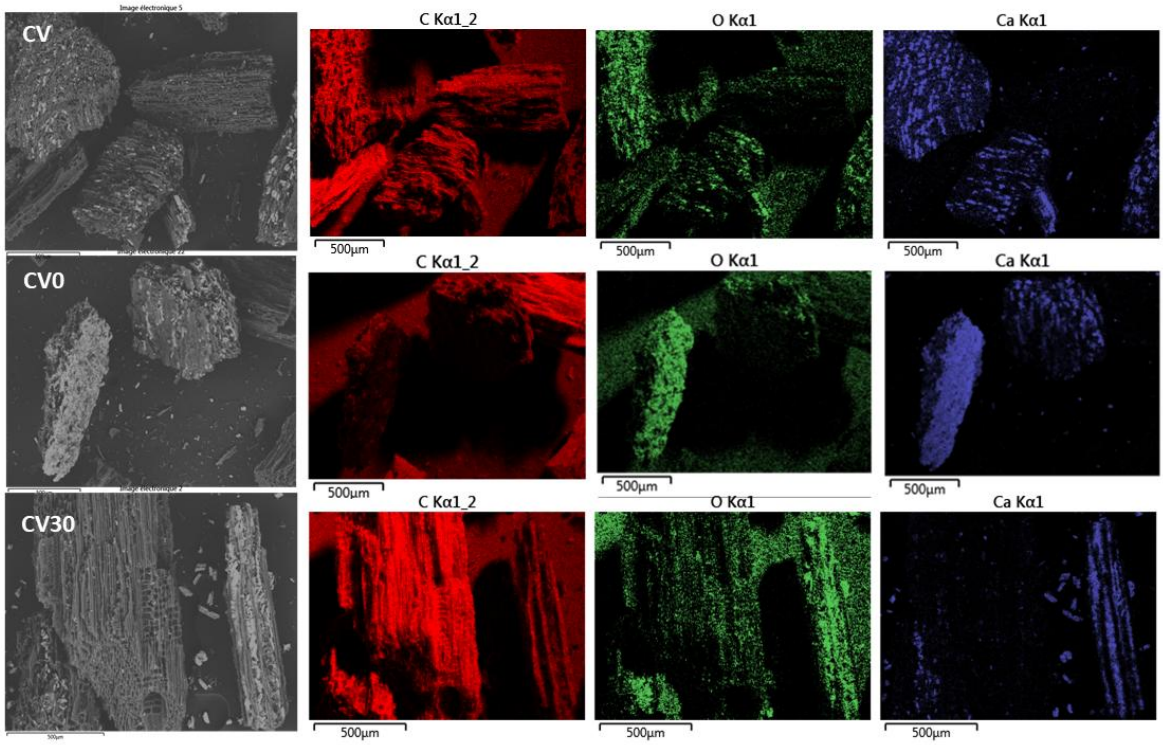

Figure 2

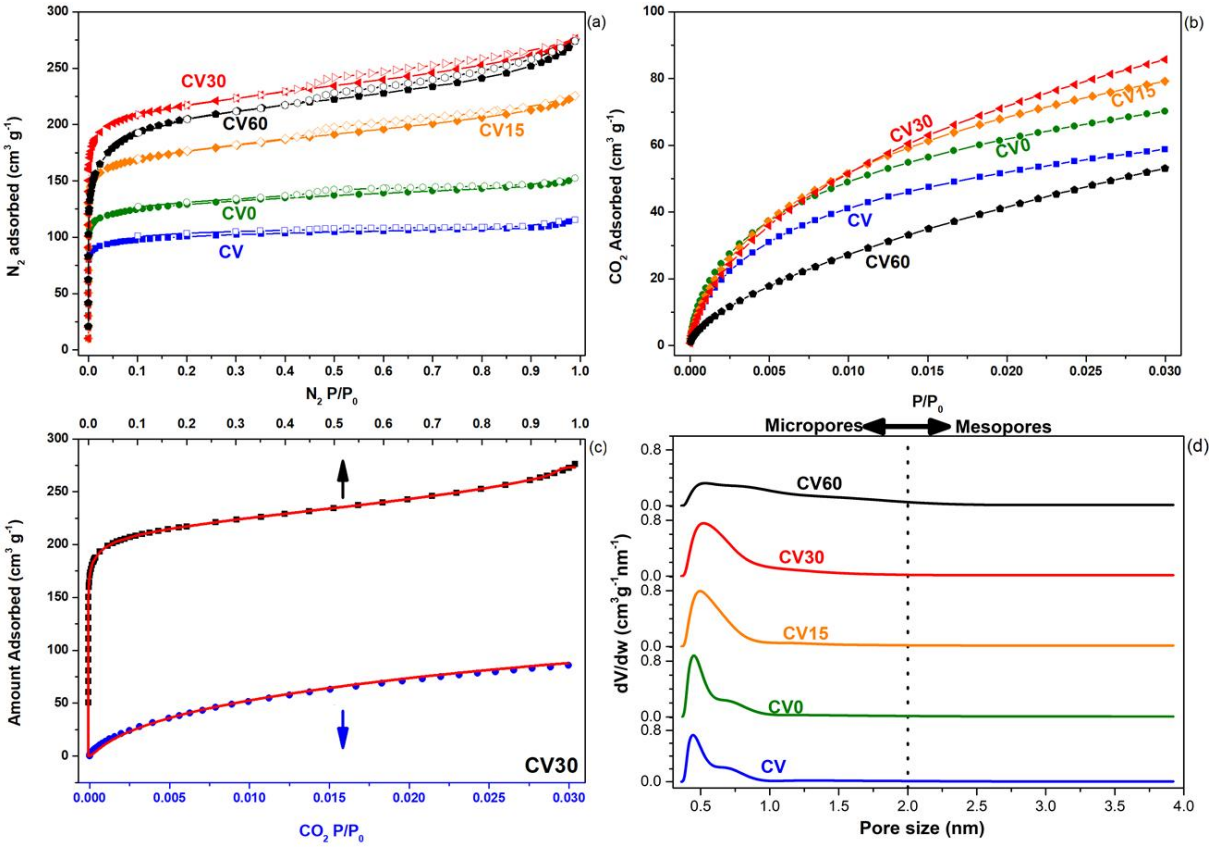
(a)
CV30
CV60
CV15
CV0
CV
N2 adsorbed (cm3 g-1)
N2 P/P0
(b)
CV30
CV15
CV0
CV
CV60
CO2 Adsorbed (cm3 g-1)
P/P0
(c)
CV30
Amount Adsorbed (cm3 g-1)
CO2 P/P0
(d)
Micropores
Mesopores
CV60
CV30
CV15
CV0
CV
dV/dw (cm3g-1nm-1)
Pore size (nm)

Figure 3

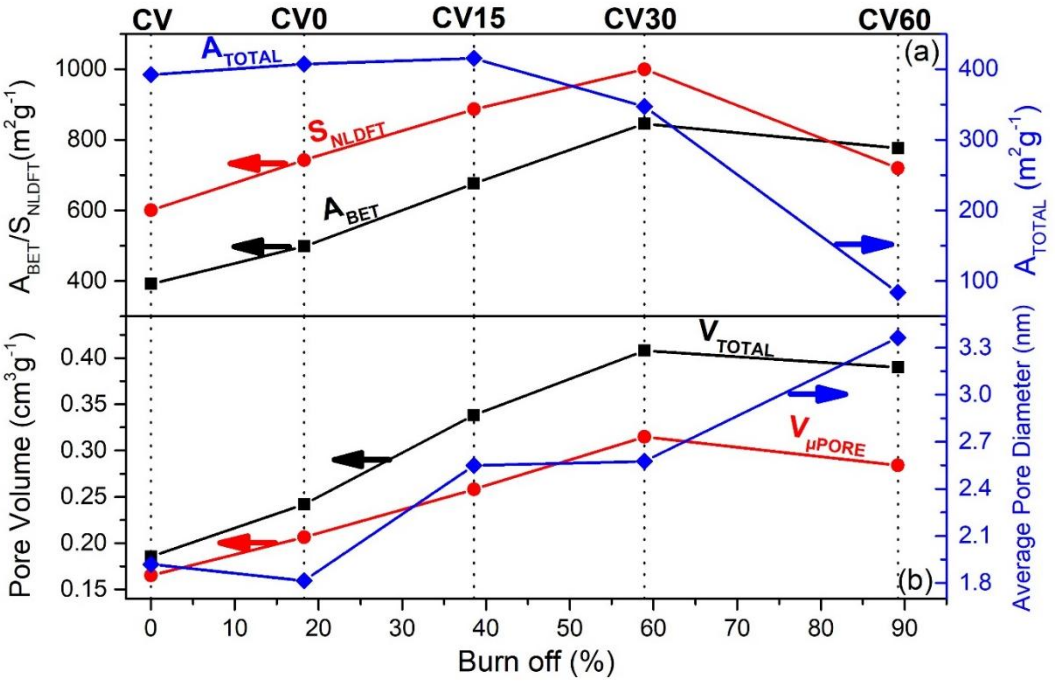
CV
CV0
CV15
CV30
CV60
A_TOTAL
S_NLDFT
A_BET
(a)
A_BET/S_NLDFT (m²g⁻¹)
A_TOTAL (m²g⁻¹)
V_TOTAL
V_μPORE
(b)
Pore Volume (cm³g⁻¹)
Average Pore Diameter (nm)
Burn off (%)

Figure 4

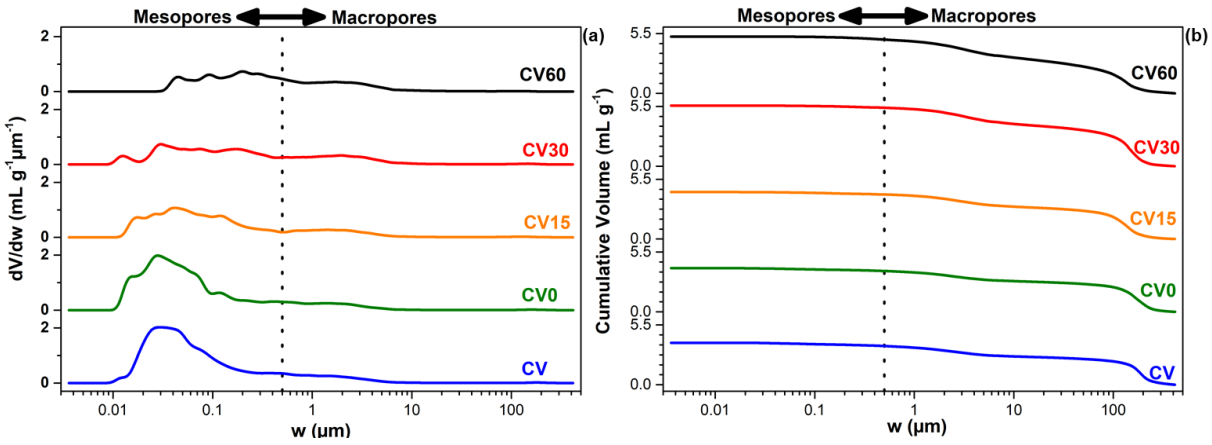
Mesopores
Macropores
(a)
dV/dw (mL g-1µm-1)
CV60
CV30
CV15
CV0
CV
w (µm)
(b)
Cumulative Volume (mL g-1)

Figure 5

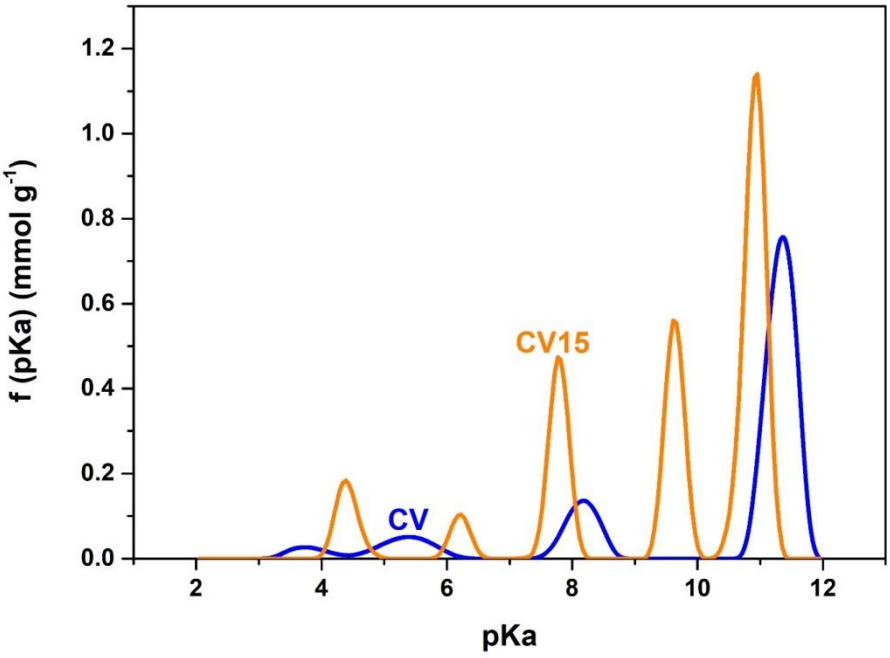

Figure 6

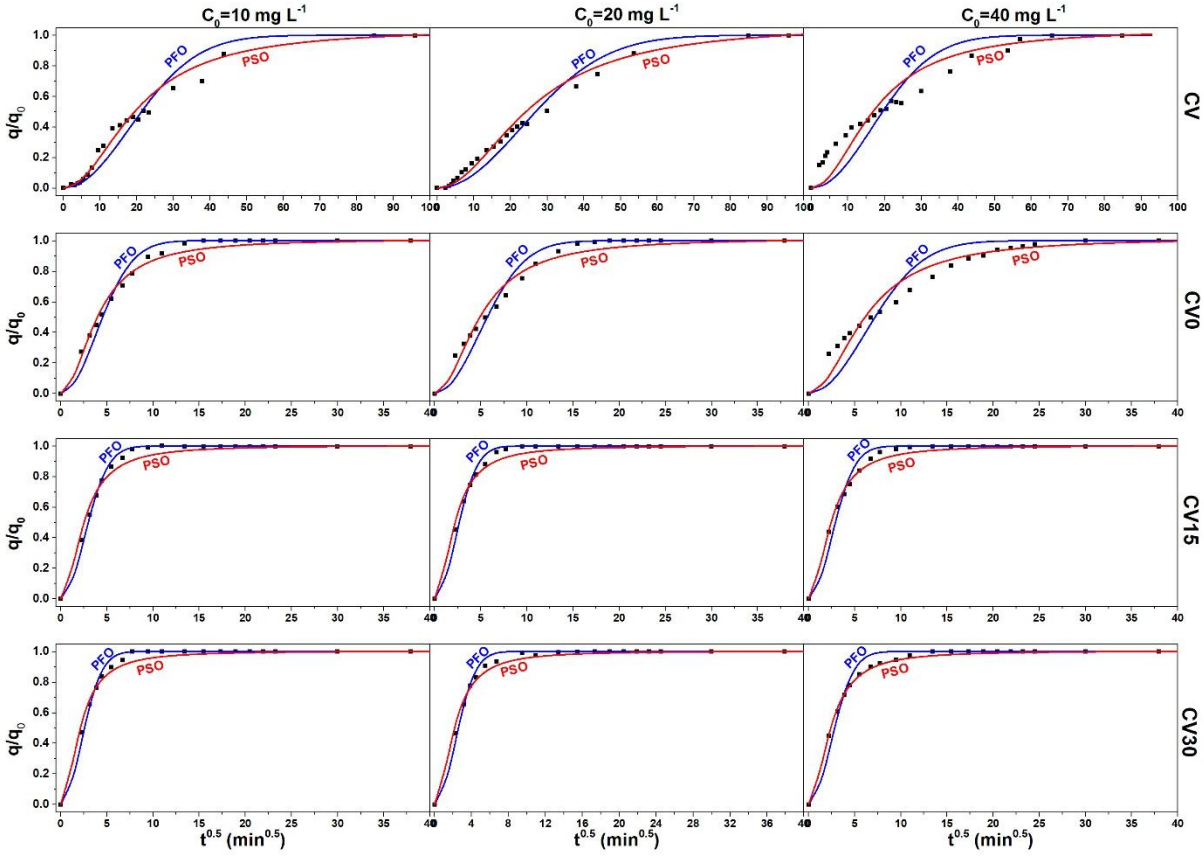
C0=10 mg L-1
C0=20 mg L-1
C0=40 mg L-1
CV
CV0
CV15
CV30
PFO
PSO
q/q0
t0.5 (min0.5)

Figure 7

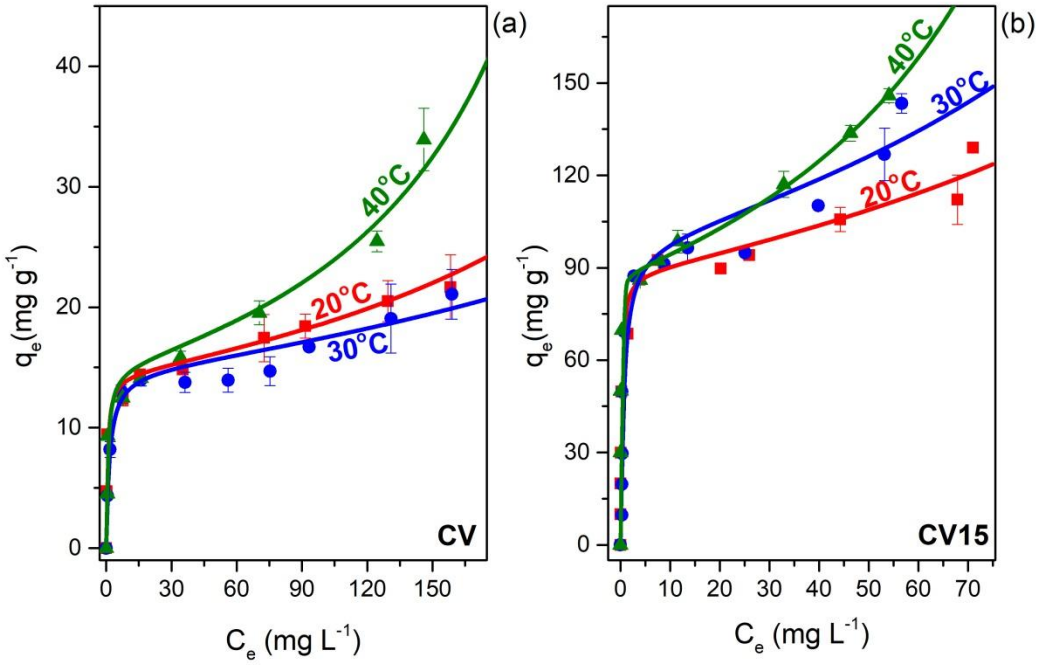
(a)
(b)
CV
CV15
40°C
30°C
20°C
q_e(mg g^{-1})
C_e (mg L^{-1})
0
10
20
30
40
60
90
120
150
50
70

Figure 8

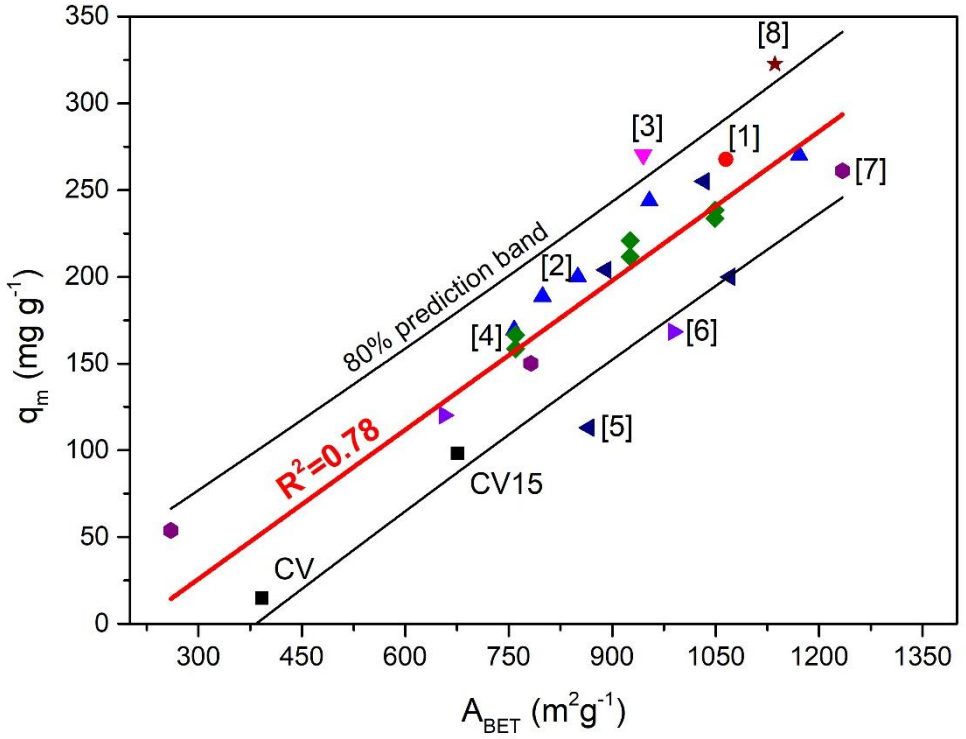
350
300
250
200
150
100
50
0
300
450
600
750
900
1050
1200
1350
q_m (mg g^{-1})
A_{BET} (m^2g^{-1})
80% prediction band
R^2=0.78
[1]
[2]
[3]
[4]
[5]
[6]
[7]
[8]
CV
CV15